

doi: 10.15407/ujpe61.03.0265

D.O. KHARCHENKO, V.O. KHARCHENKO, A.I. BASHTOVA

Institute of Applied Physics, Nat. Acad. of Sci. of Ukraine  
(58, Petropavliv'ska Str., Sumy 40030, Ukraine; e-mail: dikh@ipfcentr.sumy.ua)**SELF-ORGANIZATION  
OF AN ENSEMBLE OF VACANCIES  
UNDER THE SPINODAL DECOMPOSITION  
OF BINARY SYSTEMS AT CONTINUOUS IRRADIATION**PACS 05.40.-a, 61.72.-y,  
81.16.Rf

---

*The redistribution processes of non-equilibrium vacancies under the spinodal decomposition in a continuously irradiated solid solution have been considered. The consideration is carried out in the framework of the generalized Cahn–Hilliard model, which makes allowance for the structural disorder formation under irradiation. As the defect production rate increases, the spinodal decomposition processes are found to transform into the processes of vacancy pattern formation. It is shown that the formation of vacancy clusters is accompanied by the pattern selection processes. The decomposition and patterning kinetics, as well as the statistical distributions of solute and vacancy concentrations at various dose rates are studied.*

*Keywords:* Cahn–Hilliard model, spinodal decomposition in binary systems.

**1. Introduction**

While considering the processes of microstructural transformations in alloys subjected to irradiation, there arises an important issue concerning the behavior of an ensemble of defects, in particular, point ones. Experimental and theoretical researches of the rearrangements of vacancies and interstitial sites demonstrate that, at certain radiation exposure doses, those defects can self-organize into the so-called spatial patterns. Among them, the aggregates of vacancies (di-, tri-, and tetra-vacancies) [1], separate voids, and void lattices [2,3] can be distinguished. In addition, precipitation, defect wall formation [4], vacancy loop ordering [5,6], and some other phenomena become possible.

The majority of defects created by an external action are thermodynamically unstable and, consequently, their uniform distribution also becomes unstable. This fact results in the self-assembling of defects accompanied by the emergence of dissipative structures.

Since the mobility of interstitial sites considerably exceeds that of vacancies, interstitial atoms quickly migrate to sinks, and the number of their clusters is much smaller than the number of clusters of vacancies. Accordingly, the formation of a considerable number of vacancy patterns results in the worsening of mechanical properties of materials; e.g., in the swelling and crumbling of irradiated alloys. In this connection, the study of the vacancy subsystem dynamics in both one-component crystalline systems and multi-component ones (steels) becomes an important task.

It was found experimentally and theoretically (numerical simulation) that the dynamics of an ensemble of defects and the properties of the created defect patterns depend on irradiation conditions (the dose rate and the temperature) [7, 8]. This dependence is explained, first of all, by a reduction of the diffusion component contribution, when the defect distribution in the system is obtained by the irradiation on accelerators in comparison with the case of reactor irradiation conditions [9, 10]. As a rule, the processes of defect generation in cascades, defect annealing, and

defect cluster formation are simulated in theoretical researches by molecular dynamics methods. The dynamics of defects and their redistribution on the diffusion time scale can be examined, by using the phase-field crystal method (see, e.g., works [11, 12]). On the other hand, the effects of defect generation, migration to sinks, interaction, and diffusion can be studied at the mesoscopic level in the framework of the quasi-chemical reaction rate theory [8, 13–17]. In the framework of this approach, where the analyzed ensemble of defects is described by equations of the reaction-diffusion type for the concentration of point defects, it becomes possible to reveal specific features in the change of the defect pattern type [18], to study the dynamic and statistical properties of a defect redistribution and their dependence on irradiation conditions [9, 10], and to reveal the influence of fluctuation components on the patterning [19]. In addition, according to works [20–22], this approach together with the nucleation theory were used to explain the abnormal dynamics of grain growth in irradiated systems, when the vacancies go beyond the grain boundaries [23].

The application of this approach to the study of binary alloys allows the effects of defect self-organization into patterns in the course of phase precipitation processes at the spinodal decomposition to be analyzed in the framework of the Cahn–Hilliard theory [24] and taking Darken’s scheme [25] into account. Darken’s assumption consisting in that only the equilibrium vacancies are available can be generalized to the case of irradiation taking the rate theory into consideration. The influence of non-equilibrium vacancies on the phase separation processes was studied in works [26–30]. Darken’s approximation was demonstrated to be valid, if the diffusion length substantially exceeds the mean free path of vacancies. It was established that, in real alloys undergoing the spinodal decomposition, the diffusion length (the period of a lamellar structure at the initial decomposition stage; it is equal to about  $10^{-8}$  m) is substantially shorter than the mean free path of vacancies (about  $10^{-7}$ – $10^{-6}$  m). Therefore, the description of the phase precipitation should made allowance for the contribution of non-equilibrium vacancies at their distribution between the lamellae owing to the discrepancy between the atomic self-diffusion coefficients of alloy components. It is of importance that, in the system under irradiation, the non-equilibrium vacancies will always be created as a result of the structural dis-

order generation (radiation-induced damages). Those vacancies are directly accounted for with the help of the rate theory.

Studying the redistribution of vacancies in the system that reached a certain concentration of radiation-induced damages remains rather a challenging problem at present. Its solution in the case of one-component system was discussed in works [9, 10, 18, 19, 23], where the supersaturation with vacancies was shown to result in their assembling into stable spatial patterns. The slow-down of the decomposition process in non-irradiated systems at its initial stage by non-equilibrium vacancies was studied in work [30]. However, no scenario was proposed there for the spinodal decomposition and the self-organization in the vacancy subsystem under constant irradiation. Therefore, this work is aimed at developing the Cahn–Hilliard approach by considering the kinetics of point defects produced in cascades, as well as their redistribution with the formation of dissipative patterns. In our research, the Cahn–Hilliard theory is generalized, by introducing “quasi-chemical” reactions of defects and by assuming an interaction between vacancies in the fields of elastic stresses induced by the defects themselves. We will demonstrate that the ordinary decomposition processes take place at low irradiation doses. For slightly higher dose rates (increase in the number of non-equilibrium vacancies), the decomposition processes are slowed down, whereas, at high dose rates, the vacancies are capable of forming spatial patterns and changing the lamella morphology. We will show that processes of pattern selection become possible in this system, when the irradiation dose rate grows. We will also analyze the results of numerical simulations and find differences between the vacancy redistributions obtained at various dose rates.

The structure of the work is as follows. In Section 2, a model of the examined system is proposed, and the basic assumptions are discussed. In Section 3, the stationary states and their stability are analyzed, and the conditions for the processes of pattern selection are determined. The results of numerical simulations are discussed in Section 4. Conclusions are made in the final section of the work.

## 2. Master Equations

Let us consider a binary crystalline system composed of atoms A and B with the concentrations  $c_A$  and  $c_B$ , respectively ( $c_A + c_B = 1$ ). When constructing a

model of the system, we proceed from the definition of corresponding diffusion fluxes for each of the solid solution components,  $\mathbf{j}_{\{A,B\}} = -L_{\{A,B\}}\nabla\mu_{\{A,B\}}$ , where each of the quantities  $\mu_{\{A,B\}}$  is associated with the corresponding chemical potential for atoms of the definite sort (A or B),  $L_{\{A,B\}} = c_{\{A,B\}}D_{\{A,B\}}^*/T$  are the transport coefficients for atoms A and B,  $D_{\{A,B\}}^*$  are their self-diffusion coefficients, and  $T$  is the temperature in energy units. The main assumption consists in a substantial difference between the self-diffusion coefficients for the atoms of two sorts, i.e.  $D_A^* \neq D_B^*$ .

According to the Gibbs–Duhem relation  $c_A d\mu_A + c_B d\mu_B = 0$  for the chemical potentials  $\mu_A$  and  $\mu_B$ , the diffusion fluxes can be written as follows:  $\mathbf{j}_A = c_B L_A \nabla(\mu_B - \mu_A)$  and  $\mathbf{j}_B = -c_A L_B \nabla(\mu_B - \mu_A)$ . Taking the redistribution of vacancies into account, those formula acquire the form  $\mathbf{j}_A = c_B L_A \nabla\tilde{\mu} + (c_A D_A^*/c_v)\nabla c_v$ ,  $\mathbf{j}_B = -c_A L_B \nabla\tilde{\mu} + (c_B D_B^*/c_v)\nabla c_v$ , where  $\tilde{\mu} = \partial f/\partial c - \beta_0 \nabla^2 c_B$  is a generalized chemical potential that makes allowance for non-local interactions in inhomogeneous alloys. Here, the free energy density  $f$  is taken according to the Bragg–Williams theory of regular solid solutions. In this approximation, we have the standard expression  $f = Zw_0 c_A c_B / 2 + T(c_A \ln c_A + c_B \ln c_B)$ , where  $Z$  is the coordination number, and the ordering energy  $w_0 \equiv 2V_{A,B} - V_{A,A} - V_{B,B}$  is expressed in terms of the interaction energies  $V_{A,A}$ ,  $V_{B,B}$ , and  $V_{A,B}$ . The constant factor  $\beta_0$  in front of the squared gradient of concentration determines the squared interaction radius (the width of the interface between the phases) expressed in terms of the Fourier transform of the atom-to-atom interaction energy,  $v(k)$ , in accordance with the Krivoglaz–Clapp–Moss expression  $\beta_0 = \frac{1}{2} \frac{dv(k)}{dk^2}$ . The diffusion flux of vacancies is determined by the condition of flux conservation  $\mathbf{j}_A + \mathbf{j}_B + \mathbf{j}_v = 0$ , which makes it possible to write that  $\mathbf{j}_v = (c_A L_B - c_B L_A)\nabla\tilde{\mu} - c_v^{-1}(c_A D_A + c_B D_B)\nabla c_v$ . Owing to the Kirkendall effect, the difference between the atomic self-diffusion coefficients invokes the motion of the lattice at a rate determined by the vacancy flux  $\mathbf{j}_v$ . Therefore, in what follows, we choose the laboratory reference frame and rewrite the atomic flux in the form  $\mathbf{J}_B = \mathbf{j}_B + c_B \mathbf{j}_v$ . Substituting the expressions for the fluxes  $\mathbf{j}_B$  and  $\mathbf{j}_v$ , we arrive at the known expressions [26, 30]

$$\mathbf{J}_B = -\frac{c_A c_B (c_A D_B^* + c_B D_A^*)}{T} \nabla\tilde{\mu} +$$

$$\begin{aligned} & + \frac{c_A c_B (D_B^* - D_A^*)}{c_v} \nabla c_v, \\ \mathbf{j}_v & = \frac{c_A c_B (D_B^* - D_A^*)}{T} \nabla\tilde{\mu} - \mathcal{D}_v \nabla c_v, \\ \mathcal{D}_v & \equiv \frac{c_A D_A^* + c_B D_B^*}{c_v}. \end{aligned} \quad (1)$$

Here, the notation  $\mathcal{D}_v$  was introduced for the diffusion coefficient of vacancies, which depends on the vacancy concentration and the concentrations of the solid solution components. The cross terms in Eq. (1) describe the exchange influence on the redistribution of solution components and vacancies, respectively. Under normal conditions, the dynamics of the  $c_B$  and  $c_v$  fields are conserved, being described by the continuity equations  $\partial_t c_B = -\nabla \cdot \mathbf{J}_B$  and  $\partial_t c_v = -\nabla \cdot \mathbf{j}_v$ . In addition, in general, the vacancy concentration is supposed to be a quick mode in comparison with the solution concentration.

When considering a binary system under irradiation, we must consider the effects associated with the generation of point defects in cascades, their relaxation at sinks, and annihilation. In the defect dynamics, those effects are made allowance for in the form of “quasichemical reactions”, provided that the atomic fractions  $c_A$  and  $c_B$  must be preserved<sup>1</sup>.

The corresponding equations for the point defect dynamics are generalized by introducing the reaction components responsible for defect sources and sinks, as well as defect annihilation, into consideration. Hence, in addition to vacancies, which can interact with one another in the case of their supersaturation, by forming clusters, the model must include the interstitial atoms of two sorts with the concentrations  $c_i^A$  and  $c_i^B$ . As a result, if the processes indicated above are taken into consideration in the framework of the rate theory [8, 13–17], the evolution of the whole system will be described by the following system of equations:

$$\begin{aligned} \partial_t c_i^A & = K c_A - \mathcal{D}_i \rho c_i^A - \alpha (c_v - c_v^0) c_i^A - \nabla \cdot \mathbf{J}_i^A, \\ \partial_t c_i^B & = K c_B - \mathcal{D}_i \rho c_i^B - \alpha (c_v - c_v^0) c_i^B - \nabla \cdot \mathbf{J}_i^B, \\ \partial_t c_v & = K - \mathcal{D}_v \rho (c_v - c_v^0) - \\ & - \alpha (c_v - c_v^0) (c_i^A + c_i^B) - \nabla \cdot \mathbf{J}_v, \\ \partial_t c_B & = -\nabla \cdot \mathbf{J}_B. \end{aligned} \quad (2)$$

<sup>1</sup> If the generation of vacancies under irradiation is taken into account, the conservation law  $c_A + c_B + c_v = \text{const}$ , which is obeyed in the equilibrium case, becomes violated, because  $\int c_v(\mathbf{r}, t) d\mathbf{r} \neq \text{const}$ . In other words, the vacancy dynamics is non-conserved.

In the equations of defect evolution, the first terms characterize the defect generation at the rate of radiation-induced damages  $K$  measured in the displacement per atom per second (dpa/s) units. The second terms describe the migration of defects to sinks (these are dislocations with the concentration  $\rho$  that are “smeared” over the system) characterized by the diffusion coefficients  $\mathcal{D}_i = \epsilon \mathcal{D}_v$ , where the parameter  $\epsilon \gg 1$  involves the difference between the diffusion coefficients for vacancies and interstices. The annihilation of vacancies and interstices is determined by the recombination coefficient  $\alpha = 4\pi r_0(\mathcal{D}_i + \mathcal{D}_v)/\Omega$ , where  $r_0$  is the interaction radius, and  $\Omega$  the atomic volume (at  $\epsilon \gg 1$ , we may consider that  $\alpha \simeq 4\pi r_0 \mathcal{D}_i/\Omega$ ). The quantity  $c_v^0$  is the equilibrium concentration of vacancies.

In the last equation, the components responsible for the reactions, when the local concentration of the substance diminishes, are omitted. For example, when an interstitial atom is formed, or an atom escapes from a sink, or an interstitial atom transits into a proper site position in the lattice owing to its interaction with a vacancy. Those effects are supposed to take place at distances considerably shorter than the size of a spatial cell, in which the substance concentration is recalculated, and the processes themselves are rapid in comparison with the diffusion. That is why they can be neglected.

The last terms in Eqs. (2) characterize the corresponding diffusion fluxes. Since the diffusion coefficients of interstitial sites and vacancies were adopted to differ substantially from each other, we may consider the interstitial atoms to be uniformly distributed, without any loss of generality. This circumstance makes it possible to omit the last terms in the equations for  $c_i^A$  and  $c_i^B$ .

The total diffusion flux is introduced in the equation for the vacancy concentration. This parameter involves the flux  $\mathbf{j}_v$  and the flux of interacting vacancies  $\mathbf{j}_v^{\text{int}}$  emerging, when the elastic fields appear in vicinities of vacancies. This interaction is described by the well-known relation between the elastic fields and the concentration of their carriers, where the corresponding interaction potential looks like  $U = -\kappa \varpi \nabla \cdot \mathbf{u}$ . Here, the displacement vector  $\mathbf{u}$  satisfies the relation  $\nabla \cdot \mathbf{u} \propto \varpi c_v$ , where  $\kappa$  is the elastic constant, and  $\varpi$  the dilatation parameter [20, 31, 32]. Therefore, there arises an additional contribution to the vacancy flux,  $\mathbf{j}_v^{\text{int}} \equiv \mathbf{v} c_v$ , where

$\mathbf{v} = -(D_B^*/T)\nabla U$  is the flow velocity. Hereafter, the condition of self-consistency [18, 33–35] is accepted for the interaction potential:

$$U = - \int \tilde{u}(r, r') c_v(r') dr',$$

where  $-\tilde{u}(r)$  is an attractive potential, for which  $\int \tilde{u}(r) r^{2n+1} dr = 0$ . Assuming that  $c_v(r)$  changes slowly over the distance  $r_0 \simeq \Omega^{1/3}$ , we can use the expansion

$$\frac{1}{T} \int d\mathbf{r}' \tilde{u}(\mathbf{r} - \mathbf{r}') c_v(\mathbf{r}') \simeq \theta (c_v + r_0^2 \nabla^2 c_v), \quad (3)$$

where  $\theta = T^{-1} \int u(r) dr$  is a parameter describing the interaction between vacancies. The second term in Eq. (3) corresponds to the microscopic processes of vacancy interaction at a distance of the interaction radius  $r_0$ . Under normal conditions, this term is substantially smaller in comparison with the diffusion one. However, it cannot be neglected, because it prevents a divergence in this approximation, while approaching the vapor supersaturation [9, 10, 18, 19, 34].

For the further consideration, it is expedient to introduce dimensionless quantities by putting  $c \equiv c_B$ ,  $\varepsilon \equiv Z w_0/T$ ,  $\beta \equiv \beta_0/T$ ,  $\tilde{D} \equiv D_A^*/D_B^*$ ,  $t' \equiv t D_B^* \rho$ , and  $P \equiv K/D_B^* \rho$ . The spatial coordinates are defined as  $\mathbf{r}' \equiv \mathbf{r}/L_D$ , where  $L_D \equiv 1/\sqrt{\rho}$  is the diffusion length, and  $\ell \equiv r_0/L_D$ . Then, by introducing the scaling parameter  $\gamma \equiv 4\pi r_0/\Omega \rho$ , let us determine the rapid variables  $x_i^{A,B} \equiv \gamma c_i^{A,B}$ , which can be adiabatically omitted from consideration, provided the condition  $\partial_t x_i^{A,B} \simeq 0$ . Hence, by introducing  $x_v \equiv \gamma c_v$ , we obtain the expressions

$$\begin{aligned} x_i^A &\simeq \frac{P(1-c)}{\varepsilon[\tilde{D} + c(1-\tilde{D})]} \frac{x_v}{1+x_v-x_v^0}, \\ x_i^B &\simeq \frac{Pc}{\varepsilon[\tilde{D} + c(1-\tilde{D})]} \frac{x_v}{1+x_v-x_v^0}. \end{aligned} \quad (4)$$

Substituting them into the equation of vacancy evolution in system (2) and dropping the prime on the time variable, we obtain the system of equations

$$\begin{aligned} \gamma^{-1} \partial_t x_v &= \frac{P}{1+x_v-x_v^0} - [\tilde{D} + c(1-\tilde{D})] \frac{x_v-x_v^0}{x_v} - \\ &- \nabla \cdot \left\{ (1-\tilde{D})c(1-c) \left[ -\varepsilon \nabla c + \frac{\nabla c}{c(1-c)} - \beta \nabla^3 c \right] - \right. \\ &\left. - \frac{\tilde{D} + c(1-\tilde{D})}{x_v} \nabla x_v + \theta x_v \nabla (x_v + \ell^2 \nabla^2 x_v) \right\}, \end{aligned} \quad (5)$$

$$\partial_t c = \nabla \cdot \left\{ (1 - c(1 - \tilde{D})) c(1 - c) \times \right. \\ \left. \times \left[ -\varepsilon \nabla c + \frac{\nabla c}{c(1 - c)} - \beta \nabla^3 c \right] - \frac{(1 - \tilde{D})c(1 - c)}{x_v} \nabla x_v \right\}.$$

Let us take  $\Omega = 4\pi a^3/3$  and  $r_0 \simeq b/2$ , where  $a$  is the lattice constant and  $b$  the magnitude of Burgers vector, and let the parameters  $r_0 \sim 10^{-9}$  m,  $\Omega \sim 10^{-29}$  m<sup>3</sup>, and  $\rho \simeq 10^{14}$  m<sup>-2</sup>. Then we obtain  $L_D \simeq 10^{-7}$  m,  $\ell \sim 10^{-2}$ , and  $\gamma \sim 10^7$ . Therefore, the vacancy concentration  $x_v$  can be regarded as a rapid variable in comparison with the solution concentration  $c$ . The estimation of the dimensionless dose rate  $P$  made at  $K \simeq 10^{-6}$  dpa/s, a neutron flux of about  $10^{15}$  cm<sup>-2</sup>s<sup>-1</sup>, a neutron energy of about 0.5 MeV, a defect formation cross-section of  $3 \times 10^{-24}$  cm<sup>-2</sup> for metal targets (with an energy of initially knocked out atom of 22–25 eV), and a fixed temperature of about 770 K gives  $P \approx 0.01 \div 10$ . The main task of the further research is to describe the scenario of the vacancy ensemble self-organization at the spinodal decomposition in a binary solid solution at various rates of irradiation dose accumulation.

### 3. Stability Analysis for the Linearized System

Let us analyze the stability of the stationary states. For this purpose, it is worth noting that the quantity  $c$  is conserved. Therefore, its stationary value corresponds to the initial one, which was chosen from the interval  $c_0 \in (0, 1)$ . The stationary value of dimensionless vacancy concentration  $x_v^{st}$  is determined by solving the equation  $\partial_t x_v = 0$ :

$$x_v^{st} = x_v^0 - \frac{1}{2} + \frac{P}{2\mathcal{D}(c)} + \\ + \frac{1}{2} \left( 1 + \frac{P}{\mathcal{D}(c)} \left[ \frac{P}{\mathcal{D}(c)} - 2(1 - 2x_v^0) \right] \right)^{1/2}, \quad (6)$$

where the notation  $\mathcal{D}(c) \equiv \tilde{D} + c(1 - \tilde{D})$  was introduced. The dependence of the stationary vacancy concentration on  $P$  at various concentrations of component B is shown in Fig. 1, *a*.

One can see that, starting from the equilibrium value  $x_v^0$ , the quantity  $x_v^{st}$  grows by several orders of magnitude, when the dose rate increases. At the same time, a reduction in the stationary value of vacancy concentration is observed for systems with an enhanced content of the phase with B atoms. This

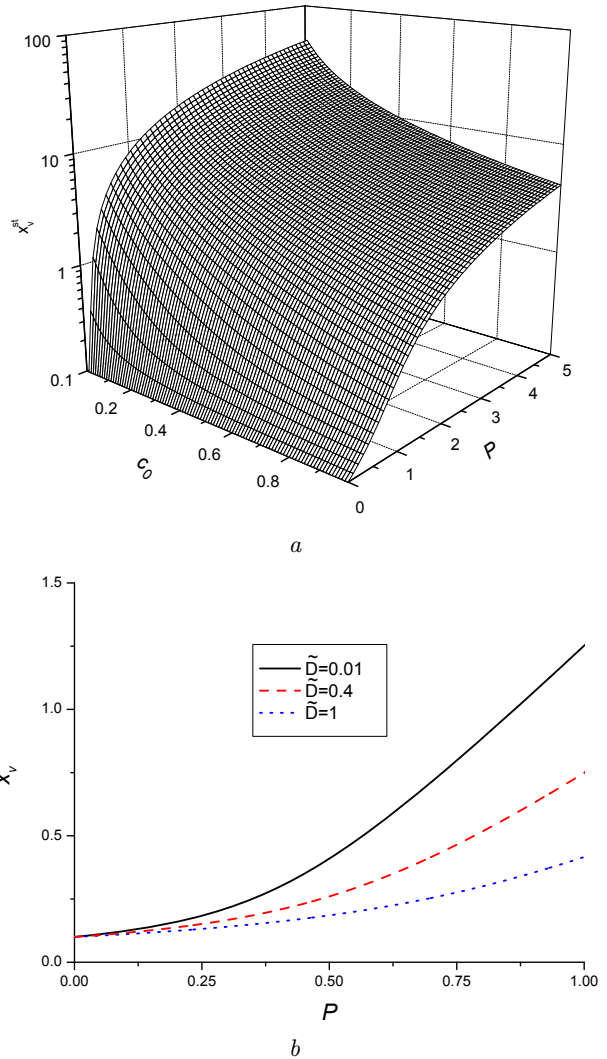


**Fig. 1.** Dependences of the stationary vacancy concentration of vacancies (*a*) on  $P$  and  $c_0$  at  $\tilde{D} = 0.1$  and (*b*) on  $P$  at various ratios  $\tilde{D} = D_A^*/D_B^*$  between the self-diffusion coefficients and  $c_0 = 1/2$

result is explained by the fact that the intensity of relaxation of non-equilibrium vacancies in phase B is considerably higher than that in phase A owing to the difference between their diffusion coefficients. The variation of the stationary vacancy concentration under irradiation of systems characterized by different  $D_A^*/D_B^*$  ratios is depicted in Fig. 1, *b*. From whence, it follows that the number of non-equilibrium vacancies is smaller in the system with a smaller difference between the self-diffusion coefficients. It is so,

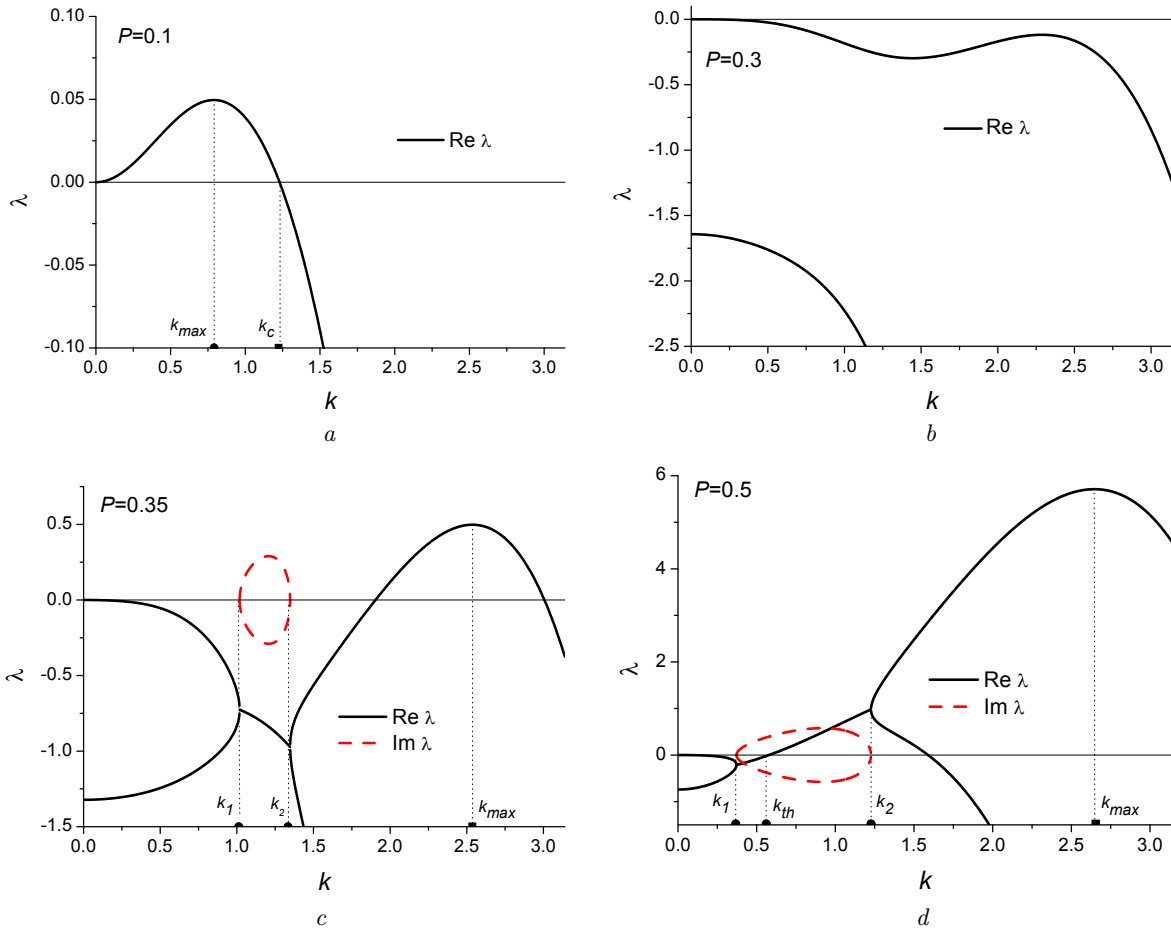


**Fig. 2.** Dependences of the characteristic values of the Jacobi matrix on the wave number in a vicinity of the stationary state ( $c_0 = 0.5, x_v = x_v^{st}$ ) at  $P = 0.1$  (a),  $0.3$  (b),  $0.35$  (c), and  $0.5$  (d). The other parameters are  $x_v^0 = 0.1, \bar{D} = 0.1, \beta = 1.0, \ell = 0.25, \varepsilon = 6,$  and  $\theta = 10$

because, in accordance with the Kirkendall effect, the vacancy flux toward the phase with a higher diffusion coefficient decreases as the self-diffusion coefficients come closer to each other.

Now, let us consider the stability of the stationary state ( $c_0, x_v^{st}$ ), by assuming the deviations  $\delta c = c_0 + e^{\lambda(k)t + i\mathbf{k}\mathbf{r}}$  and  $\delta x_v = x_v^{st} + e^{\lambda(k)t + i\mathbf{k}\mathbf{r}}$  to be small. Linearizing the system of equations (5) in a vicinity of the point ( $c_0, x_v^{st}$ ), we can obtain the characteristic values  $\lambda(k)$  of corresponding Jacobi matrix as the solutions of a quadratic equation. One of them is always negative, whereas the other can accept positive values, depending on the rate  $P$ . In addition, the complex roots of this quadratic equation are also possible. The presence of complex roots points to an os-

cillatory behavior of the concentration fields of the solution, vacancies, and corresponding structural factors as the Fourier transforms of two point correlation functions  $\langle \delta c(\mathbf{r}, t) \delta c(\mathbf{r}', t) \rangle$  and  $\langle \delta x_v(\mathbf{r}, t) \delta x_v(\mathbf{r}', t) \rangle$ . Such an oscillatory behavior testifies to a pattern selection, when, among structures with different sizes, the system selects only that which corresponds to the most unstable mode with the wave number  $k_{max}$ . In this case,  $\lambda(k_{max})$  turns out to be the maximum positive characteristic value of the stability matrix.

Let us consider the influence of the defect formation rate on the course of pattern selection processes, by analyzing the characteristic values of Jacobi matrix. The dependences  $\lambda(k)$  at various  $P$  are exhibited in Fig. 2. At  $P = 0.1$  (see Fig. 2, a), we have a single

real positive root for  $\lambda(k)$  in the interval  $0 < k < k_c$ , where  $k_c$  is the critical wave number that confines unstable modes. Hence, if the defect formation rate is low, the ordinary process of phase stratification takes place, which is observed at the decomposition of the non-irradiated system. As the defect formation rate increases owing to the structural disorder generation, the number of unstable modes considerably diminishes: the maximum of the positive characteristic value,  $\lambda(k_{\max})$ , falls down, and its position corresponding to  $k = k_{\max}$  shifts to  $k = 0$ . The latter fact testifies that only the long-wave patterns survive. At  $P = 0.3$  (see Fig. 2, b), all characteristic values of stability matrix are negative. This means that the non-equilibrium vacancies substantially hamper the decomposition at the rates concerned owing to the inverse Kirkendall effect. A further growth of  $P$  results in the appearance of positive  $\lambda(k)$ -values in a confined interval of nonzero wave numbers (see Fig. 2, c for  $P = 0.35$ ). In this case, two real negative characteristic values of Jacobi matrix degenerate, so that two complex-conjugate characteristic values emerge in a certain interval  $k_1 < k < k_2$ . Hence, at high dose rates, owing to the supersaturation with interacting vacancies, a patterning takes place, which is accompanied by the processes of pattern selection ( $\text{Im } \lambda(k) \neq 0$ ). In this case,  $\text{Re } \lambda(k) < 0$ ; therefore, the corresponding processes are damped, and, ultimately, only one unstable mode with the wave number corresponding to the maximum of  $\lambda(k)$  survives. As the defect formation rate grows further (see Fig. 2, d for  $P = 0.5$ ), the processes of pattern selection do not damp within short time intervals. This situation is characterized by the inequality  $\text{Im } \lambda(k) \neq 0$ , with  $\text{Re } \lambda(k) > 0$  in a narrow interval of wave numbers  $k_{th} < k < k_2$ , where  $k_{th}$  is the emergence threshold for unstable oscillation modes. Evidently, only those patterns will survive, the period of which will correspond to the maximum  $\lambda(k_{\max})$ .

Note that the processes of pattern selection in non-irradiated systems are strongly associated with a finite velocity of perturbation transfer; in particular, with a finite relaxation time for the diffusion flux (see works [11, 36–38]). In our case, those processes are connected with electromagnetic irradiation at high dose rates.

Now, let us consider how the dependence of the wave number  $k_{\max}$  on  $P$  changes its character for various values of the key system parameters (see

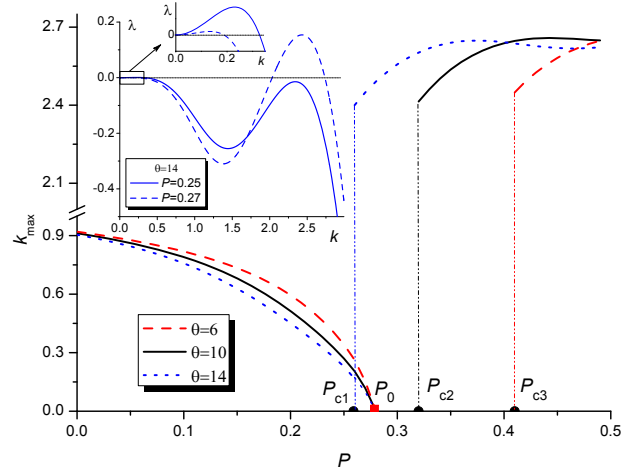


**Fig. 3.** Dependences  $k_{\max}(P)$  at various  $\varepsilon$  and  $\theta$ . The other parameters are  $c_0 = 0.5$ ,  $\varepsilon = 6$ ,  $x_v^0 = 0.1$ ,  $\tilde{D} = 0.1$ ,  $\beta = 1.0$ , and  $\ell = 0.25$

Fig. 3). The general form of the obtained dependences testifies to the following: as  $P$  grows, the system undergoes a phase stratification with the formation of long-wave patterns, lamellae ( $k_{\max} \rightarrow 0$ ); at higher dose rates, a drastic (jump-like) growth of  $k_{\max}$  is observed, which the formation of spatial clusters with a restricted characteristic length, i.e. the patterning. The reduction of  $k_{\max}$ , when  $P$  increases from zero, testifies that the phase interfaces become smeared as a result of the structural disorder generation under irradiation, and the number of vacancies is not enough for the patterning, because the required vacancy supersaturation is not attained. This effect was discussed in some previous works dealing with the phase stratification in irradiated systems (see works [38–41]).

When the vacancy supersaturation is reached (at high  $P$ ), the defects self-organize into an ensemble, which is accompanied by the formation of patterns of interacting defects. The processes of defect patterning in one-component systems subjected to irradiation were studied in works [9, 10, 18, 19], where the influence of irradiation conditions on the character of created vacancy patterns was demonstrated. A similar variation in the behavior of an irradiated system from phase stratification to patterning with a growth of the irradiation dose rate was discussed earlier, when a binary system was simulated, by using the phase field and kinetic Monte Carlo methods (see works [42–44]). It is of importance that, in this case,

there exists a certain interval for the parameters, in particular, for  $\varepsilon$  and  $\theta$ , in which the growth of the irradiation dose rate is not accompanied by the emergence of unstable modes on short-time scales. In this case, the system becomes homogeneous ( $k_{\max} = 0$ ), i.e. the phases enriched in atoms A and B are not separated, because the vacancies are generated and mixed over the whole system. Comparing the solid and dashed curves in Fig. 3, one can see that, if the dose rate does not exceed  $P = P_0$ , the stratification processes in the system with the formation of long-wave lamellae remain possible. It is evident that the vacancies will be mainly concentrated in the “soft” phase (with a higher atomic self-diffusion coefficient,  $D_B^* \gg D_A^*$ ).

As  $P$  grows further, a homogeneous state is realized at a certain critical value  $P_{c\{2,3\}}$  depending on the ratio between the interaction parameters  $\varepsilon$  and  $\theta$ . Since  $\lambda < 0$  in this case, the system is stable with respect to spatial perturbations, which allows us to put  $k_{\max} = 0$ . The growth of the interaction parameter  $\theta$  results in the narrowing of the interval, where the uniform distributions of the vacancy and solution concentrations are realized. If the ratio between  $\theta$  and  $\varepsilon$  is large, the stratification and the patterning modes change, and the homogeneous states are not realized (the dashed curve in Fig. 3). Now, the patterning threshold  $P_{c1}$  is considerably lower than the phase stratification threshold  $P_0$ . In the interval  $P_{c1} < P < P_0$ , the quantity  $\lambda$  has two peaks: one of them (at small  $k$ ) is responsible for stratifications, and the other (at large  $k$ 's) for the patterning (see the inset in Fig. 3). However, since the most unstable mode  $k_{\max}$  corresponds to the largest maximum  $\lambda$ -value, it is evident that, when approaching  $P_{c1}$ , the stratification processes will be drastically substituted by the patterning ones. According to the results obtained, the corresponding redistribution of vacancies is essentially associated with the Kirkendall effect.

#### 4. Numerical Simulation

Here, we will numerically solve the system of equations (5), in which  $t$  is the dimensionless time. The numerical solution procedure was carried out on a square  $L \times L$  mesh with the linear length  $L = N\Delta l$ , where  $N = 256$  was the number of cells, each with the characteristic length  $\Delta l = 0.25$  (the spatial step). The initial conditions were as follows:  $\langle c(\mathbf{r}, 0) \rangle = 0.5$  and  $\langle x(\mathbf{r}, 0) \rangle \equiv x_0 = 0.1$ . Periodic

boundary conditions were selected. The difference between the characteristic time scales of evolution for the solution and vacancy concentrations was fixed by the value  $\gamma = 10^3$ . The simulation was performed at  $\tilde{D} = 0.1$ ,  $\varepsilon = 6$ ,  $\beta = 1$ ,  $\theta = 10$ ,  $\ell = 0.25$ , and with the time integration step  $\Delta t = 0.00015$ .

Typical scenarios of evolution of the system at various defect formation rates  $P$  are shown in Fig. 4 (here, the upper row corresponds to the concentration field of the solution, and the lower one to the concentration field of non-equilibrium vacancies). From Fig. 4, *a*, one can see that the ordinary process of phase separation takes place in the system at low dose rates. Owing to the Kirkendall effect, the vacancies mainly migrate into the phase region, where the diffusion coefficient is higher ( $D_B^* \gg D_A^*$ ). In this case, the morphology of vacancy formations repeats the lamella morphology of precipitating phases. As  $P$  grows (see Fig. 4, *b*), the weakly pronounced patterning processes become observed in the system within short time intervals. At the same time, the domains of various phases with vacancies in the phase with the higher self-diffusion coefficient of the corresponding sort of atoms are separated on the long-time scale. At even higher rates  $P$  (see Fig. 4, *c*), the vacancy patterns are formed, and the corresponding redistribution of atoms of the solution takes place. At the supersaturation with non-equilibrium vacancies, the vacancy clusters are formed within long-time intervals in the phase with the lower self-diffusion coefficient of atoms (the “solid” phase) and at interfaces. Such a scenario is explained by the fact that the relaxation intensity of non-equilibrium vacancies is higher in the phase with a higher self-diffusion coefficient of atoms (the “soft” phase). The vacancies in the “solid” phase are less mobile, which results in their self-organization into clusters owing to the supersaturation and the interaction in this phase. In contrast, the non-equilibrium vacancies accumulated in the “soft” phase annihilate and migrate to sinks more intensively. This effect corresponds to the obtained dependence of the stationary concentration of non-equilibrium vacancies on the solution composition (see Fig. 1, *a*). It should be noted that the patterning processes run only at elevated dose rates  $P$ , which corresponds to the linear stability analysis.

According to the obtained numerical data, the processes of pattern selection can be analyzed on the short-time scale. For this purpose, the

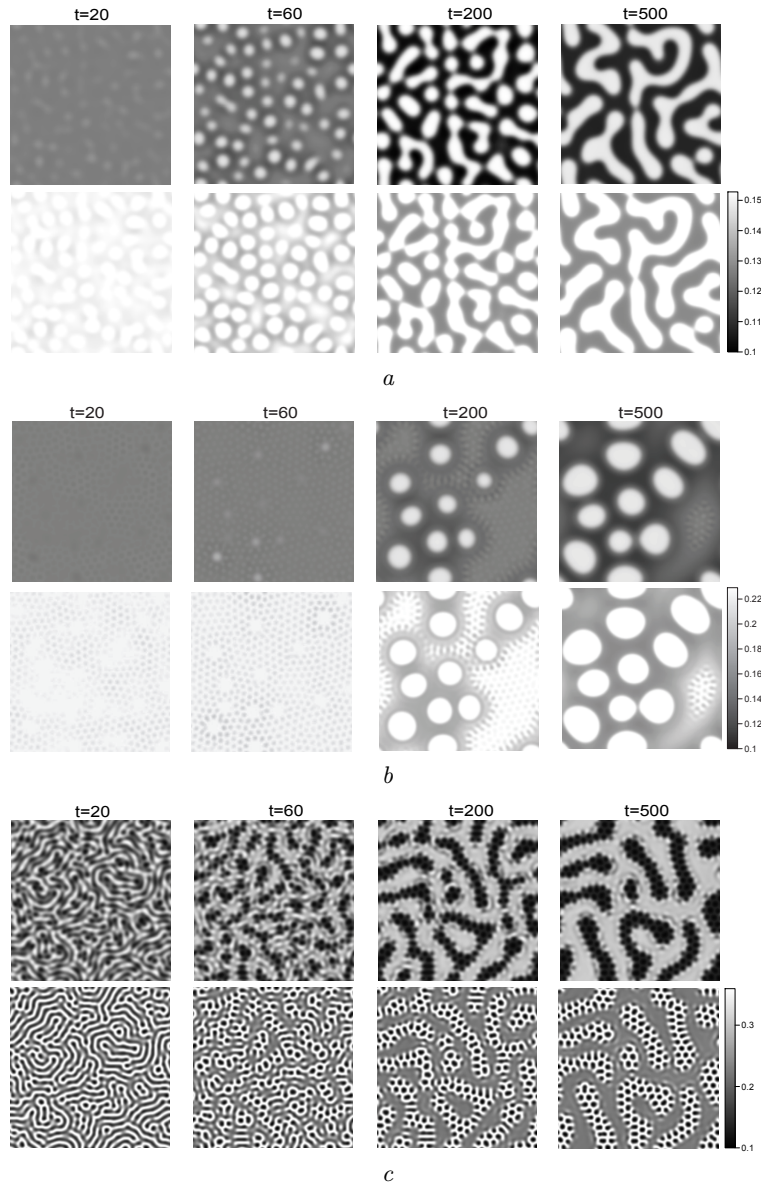


**Fig. 4.** Evolution of the solution and vacancy concentration fields at  $\tilde{D} = 0.1$  and various  $P = 0.2$  (a),  $0.35$  (b), and  $0.5$  (c)

two-point correlation function  $\langle \delta c(\mathbf{r}, t) \delta c(\mathbf{r}', t) \rangle$  is calculated, and the structure factor  $S(\mathbf{k}, t) = \int \langle \delta c(\mathbf{0}, t) \delta c(\mathbf{r}, t) \rangle e^{i\mathbf{k}\mathbf{r}} d\mathbf{r}$  is determined. The quantity  $S(\mathbf{k}, t)$  is spherically averaged by the formula  $S(k, t) = N_k^{-1} \sum_{k < |\mathbf{k}| < k + \Delta k} S(\mathbf{k}, t)$ , where  $N_k$  is the number of rings, and the width of each ring equals  $\Delta k$ . The dynamics of  $S(k, t)$  at various  $P$ -values is illustrated in Fig. 5. As follows from Fig. 5, *a*, the process of phase stratification is observed at low  $P$ :

the peak position of the structure factor tends in time to  $k = 0$ , its height increases, and phase domains are formed in the system following the spinodal mechanism. The behavior of  $S(k, t)$  at higher  $P$  differs substantially from the described case. In particular, Fig. 5, *b* demonstrates the presence of several peaks for the structure factor at various time cross-sections. The peak height grows in time at large wave numbers and diminishes at small ones. Such an

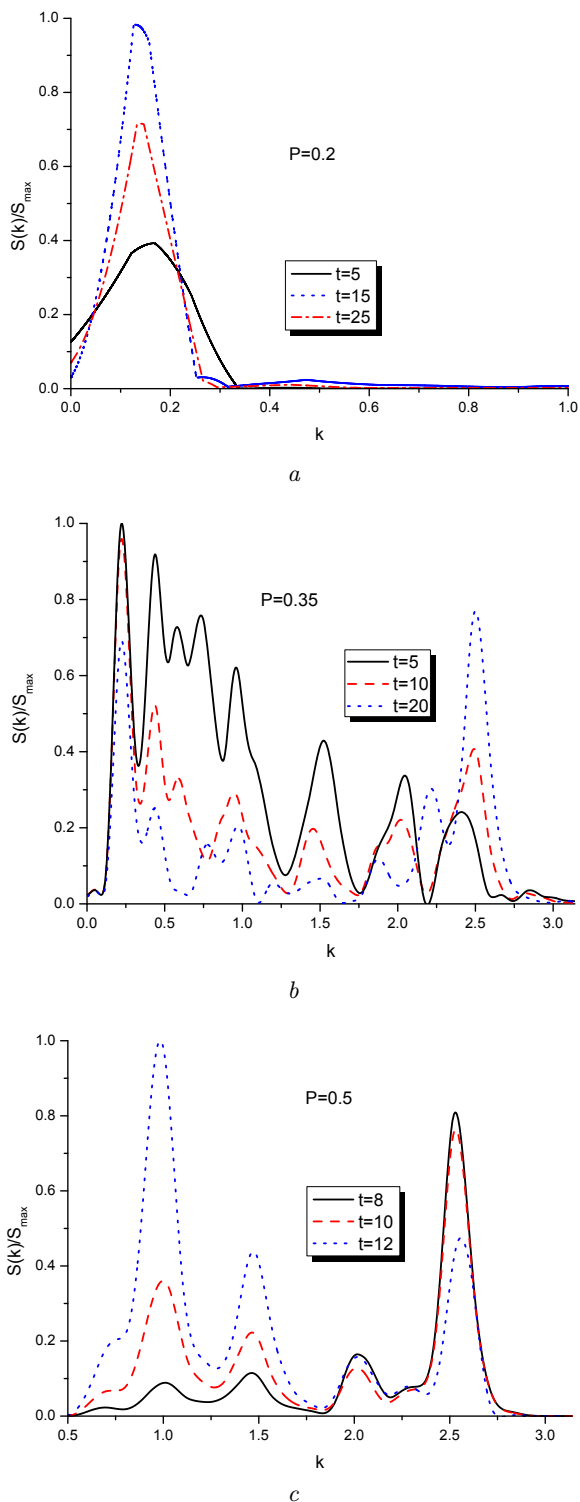


Fig. 5. Structure factor dynamics at various  $P$  at the initial stage:  $P = 0.2$  (a),  $0.35$  (b), and  $0.5$  (c)

oscillatory behavior testifies in favor of the pattern selection processes. In the course of a further evolution, the satellite peaks, which correspond to the sizes of damped patterns, disappear, so that only one peak characterizing the most unstable mode ultimately survives. A similar effect for a change in the peak height is observed in Fig. 5, *c* corresponding to  $P = 0.5$ . Here, the height of the peak at small  $k$  grows in time. The difference between those two cases ( $P = 0.35$  and  $P = 0.5$ ) is explained by the fact that, at  $P = 0.5$ , the increase in the oscillation intensity at small wave numbers is observed, which was shown in Fig. 2 at  $P = 0.5$ , when  $\text{Im } \lambda \neq 0$  and  $\text{Re } \lambda > 0$ . As the time increases, only one peak survives, which corresponds to the wave number  $k_{\max}$ .

Let us consider the ordering dynamics by analyzing  $\langle x_v(t) \rangle$ ,  $J_v(t) = \langle (\delta x_v(\mathbf{r}, t))^2 \rangle$ , and  $J_c = \langle (\delta c(\mathbf{r}, t))^2 \rangle$ . The first quantity is the average value of vacancy concentration in the system (the average solution concentration remains constant at the simulation, in accordance with the mass conservation law). The other two quantities play the role of order parameters at the patterning and the phase stratification. They describe the dispersion in the distribution of a corresponding field. The growth of the dispersion evidently testifies to the separation of aggregates (patterns, phases), i.e. to an ordering in the initially homogeneous system. The corresponding time dependences are shown in Fig. 6, *a* to 6, *c*.

In particular, the dependences  $\langle x_v(t) \rangle$  (see Fig. 6, *a*) demonstrate that the vacancy concentration first grows from the equilibrium value (vacancies are accumulated), then the vacancies migrate to sinks (a drastic drop), and a slow transition to the stationary regime occurs finally (the vacancy redistribution with the “soft” phase formation and/or the patterning). Depending on the  $P$ -value, the metastable phase existence time (while the vacancies migrate to sinks) changes. Namely, at high rates, the number of vacancies grows rapidly, and their redistribution happens instantly; at low  $P$ , this process is slowed down.

The character of the vacancy ordering can be monitored, by using the time dependences of  $J_v$ . If  $P$  is low (the solid and dashed curves in Fig. 6, *b*), the order parameter firstly decreases, which is explained by the uniform distribution of vacancies in the system. The further growth of  $J_v$  testifies to a redistribution of vacancies, with their segregation in the “soft” phase. The growth of  $P$  results in an increase of the

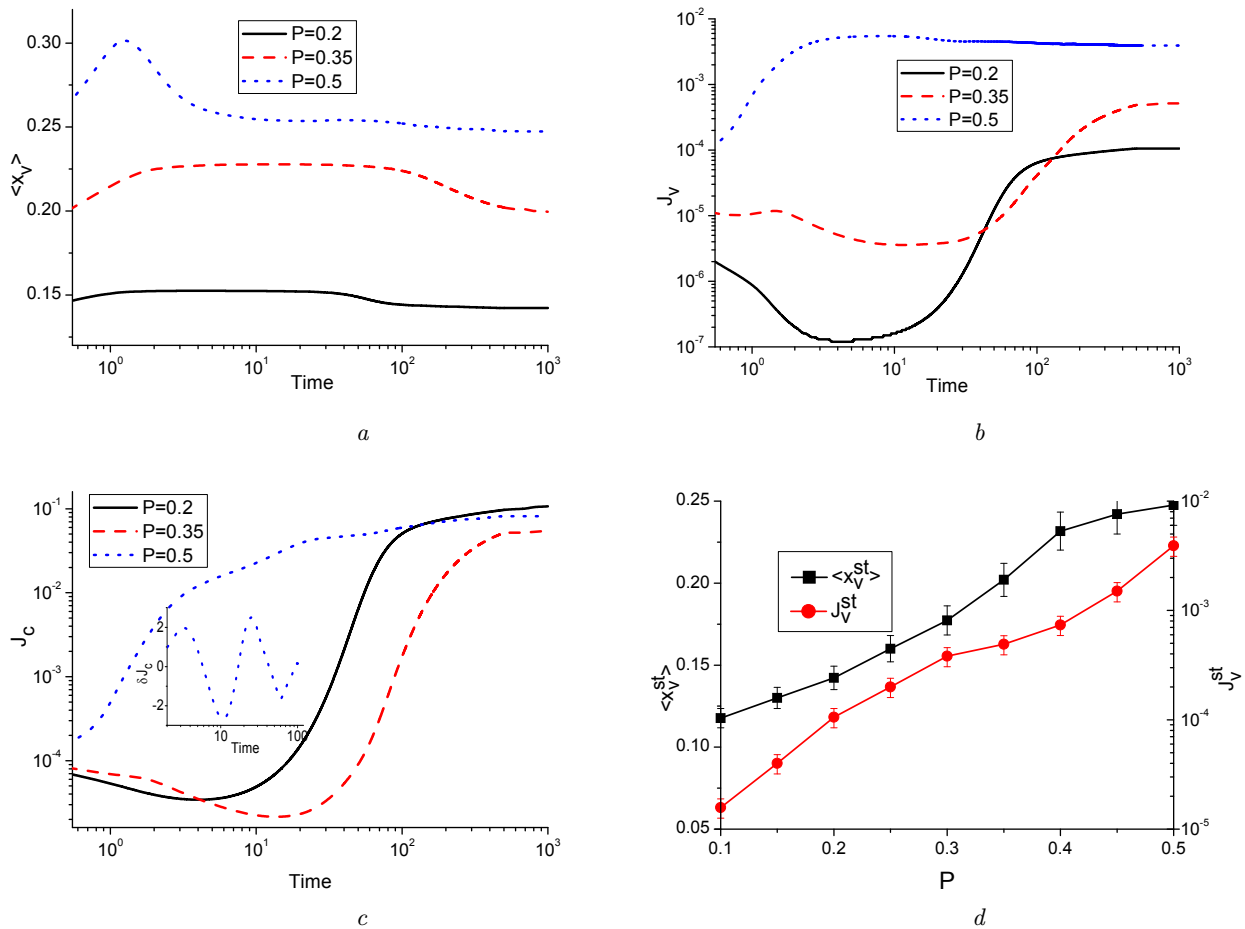


**Fig. 6.** Time dependences of the average vacancy concentration  $\langle x_v \rangle$  (a), the order parameter  $J_v$  (b), and the order parameter  $J_c$  (c). (d) Dependences of stationary  $\langle x_v^{st} \rangle$ - and  $J_v^{st}$ -values on  $P$

order parameter  $J_v$ . At  $P = 0.5$ , the essentially different dynamics of  $J_v$  is observed (see the dotted curve in Fig. 6, b). Here, the relaxation regime is realized substantially earlier and runs much more rapidly in comparison with the previous cases (not shown in the figure). The order parameter drastically grows by several orders of magnitude and transits to the stationary regime. Hence, the ordering process is substantially accelerated at high  $P$ , and it is accompanied by the patterning of non-equilibrium vacancies.

It should be noted that the order parameter  $J_v$  increases non-monotonically, when  $P$  grows. This non-monotonicity is explained by the oscillatory behavior. Really, as follows from the stability analysis in the linear approximation and the dynamics of the structure factor at initial stages, the oscillatory be-

havior should be inherent to  $J_v$  and  $J_c$ . Since the magnitude of  $J_v$  is small, the corresponding oscillations can be illustrated rather well by considering the behavior of the order parameter  $J_c$ , which is shown in Fig. 6, c. Here,  $J_c$  expectedly grows, which points to the phase precipitation. In due time, those phases have to divide the whole system into two equivalent ones. Therefore, the value of  $J_c$  will grow logarithmically slowly at large times. The process of pattern selection and the corresponding oscillations can be seen at the growing and coarsening stages, provided that a corresponding trend is subtracted from the  $J_c$ -dependence (at  $P = 0.5$ ). As a result, we obtain the quantity  $\delta J_c$ , whose dynamics explicitly illustrates the oscillatory character of selection processes (see the inset in Fig. 6, c).

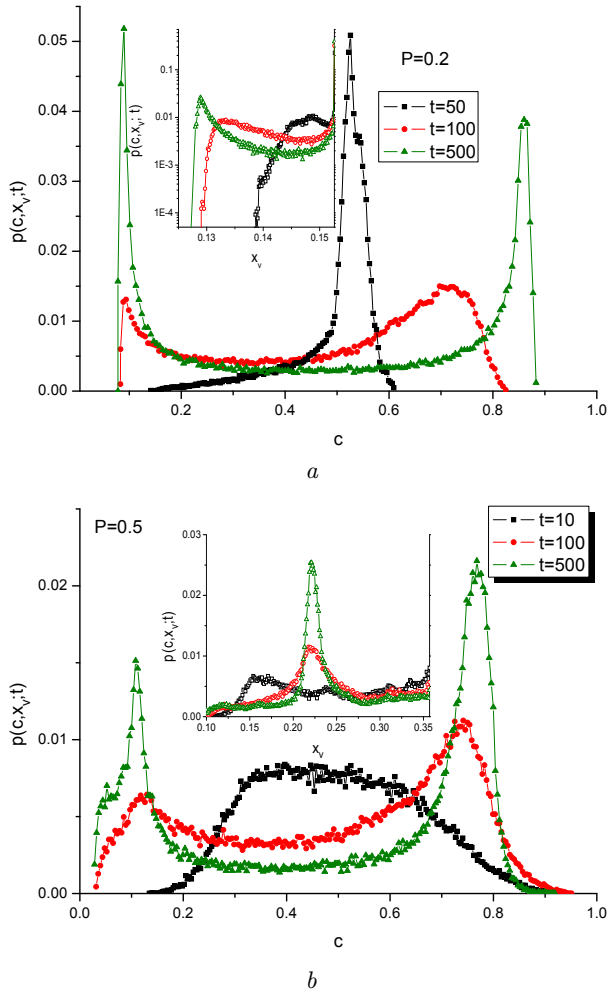


**Fig. 7.** Dynamics of the distribution functions for  $c$ - and  $x_v$ -values at  $P = 0.2$  (a) and  $0.5$  (b)

The influence of the defect formation rate on the stationary values of average vacancy concentration and corresponding order parameter is illustrated in Fig. 6, *d*. One can see that the growth of  $P$  increases the  $\langle x_v^{st} \rangle$ -value and enlarges the order parameter  $J_v^{st}$  by several orders of magnitude. We should emphasize that the growth of the rate  $P$  substantially slows down the process of spinodal decomposition (cf. curves  $J_c(t)$  at  $P = 0.2$  and  $0.35$ ). Moreover, in the case  $P = 0.3$ , no spatial instability arises in the system at all. Such a damping is associated, first of all, with the inverse Kirkendall effect, when the non-equilibrium vacancies slow down phase separation processes [45]. The further growth of  $P$  results in the supersaturation of non-equilibrium vacan-

cies, which gives rise to their interaction and patterning. At high rates ( $P = 0.5$ ), the order parameter  $J_c$  drastically grows, which is a “smoking gun” of rapid patterning processes.

Finally, let us analyze the evolution of the distribution functions  $p(c, x_v; t)$  for the solution and vacancy concentrations at various dose rates. The corresponding dependences are exhibited in Fig. 7. The general character of the solution concentration field distribution is as follows. On a short-time scale, the unimodal distribution of the solution concentration becomes smeared in a vicinity of the initial concentration  $c_0 = 0.5$ . Afterward, this distribution becomes bimodal; two phases precipitate, which are enriched in atoms of sort A or B. Depending on the accumulated dose, the properties of this smearing and the formation of a bimodal distribution differ only in detail. At the same time, the distributions of the vacancy concentration are considerably different at low and high  $P$ , which is illustrated in the insets in Fig. 7. In particular, at low  $P$  (see the inset in Fig. 7, *a*), the unimodal distribution is transformed into a bimodal one on long-time scale. This means that vacancy-depleted and vacancy-enriched regions become separated in the course of evolution of the system. This scenario is typical at those defect formation rates, when the stratification processes are still observed in the system. As  $P$  grows (see the inset in Fig. 7, *b*), and the patterning takes place, the initial unimodal distribution of vacancies becomes essentially smeared even on a short-time scale. On a long-time scale, it transforms into a unimodal one in a much wider interval of vacancy concentrations in comparison with the previous two intervals. The appearance of a single peak in the corresponding distribution testifies to the precipitation of the phase with vacancy patterns. The latter are so arranged in the “solid” phase that the vacancy distribution is only weakly smeared near the phase interfaces and in the other phase.

## 5. Conclusions

In the framework of a generalized model for the redistribution of non-equilibrium vacancies at the spinodal decomposition of a binary solid solution subjected to constant irradiation, the influence of the defect formation rate on the defect pattern self-organization

has been studied. At high defect formation rates, the process of spinodal decomposition is found to be hindered by residual non-equilibrium vacancies and to transform into the process of vacancy patterning. The formation of vacancy clusters at high formation rates of radiation-induced damages is accompanied in this case by a pattern selection at the initial stages. The analysis of the ordering dynamics has shown that the non-equilibrium distribution of vacancies results in a deceleration of spinodal decomposition processes according to the inverse Kirkendall effect. The statistical analysis of the distributions of non-equilibrium vacancies at the spinodal decomposition and the patterning reveals that, in the former case, the non-equilibrium vacancies are mainly concentrated in the lamellae consisting of the “soft” phase, in which the self-diffusion coefficient of atoms is higher than that in the other phase. In the course of patterning, the interaction of vacancies in their supersaturated solution results in the formation of vacancy clusters in the lamellae of “solid” phase and at the interfaces. At the same time, the vacancy distribution in the lamellae of the other phase is smeared.

The authors believe that the obtained theoretical results can be used for the explanation of the spinodal decomposition in binary systems (alloys) and the defect patterning processes under various irradiation conditions. We also hope for that they can stimulate relevant experimental researches in this direction, while developing new constructional materials.

1. J.H. Evans, *Nature* **229**, 403 (1971).
2. S. Saass and B.L. Eyre, *Phil. Mag.* **27**, 1447 (1973).
3. P.B. Johnson, D.J. Mazey, and J.H. Evans, *Radiat. Eff.* **78**, 147 (1983).
4. J.E. Evans and D.J. Mazey, *J. Nucl. Mater.* **138**, 176 (1986).
5. A. Jostobns and K. Farrel, *Radiat. Eff.* **15**, 217 (1972).
6. J.O. Steigler and K. Farrel, *Scripta Metall.* **8**, 651 (1974).
7. V.N. Voevodin and I.M. Neklyudov, *Structural-Phase State Evolution and Radiation Resistance of Structural Materials* (Naukova Dumka, Kyiv, 2006) (in Russian).
8. D. Walgraef, *Spatio-Temporal Pattern Formation* (Springer, New York, 1996).
9. D.O. Kharchenko, V.O. Kharchenko, and A.I. Bashtova, *Ukr. J. Phys.* **58**, 993 (2013).
10. D.O. Kharchenko, V.O. Kharchenko, and A.I. Bashtova, *Radiat. Eff. Defects Solids* **169**, 418 (2014).
11. D. Kharchenko, V. Kharchenko, and I. Lysenko, *Centr. Eur. J. Phys.* **9**, 698 (2011).
12. D.O. Kharchenko, V.O. Kharchenko, S.V. Kokhan, and I.O. Lysenko, *Ukr. J. Phys.* **57**, 1069 (2012).
13. G. Martin, *Phys. Rev. B* **30**, 1424 (1984).
14. C. Abromeit and G. Martin, *J. Nucl. Mater.* **271–272**, 251 (1999).
15. N.M. Ghoniem and D. Walgraef, *Model. Simul. Mat. Sci. Eng.* **1**, 569 (1993).
16. D. Walgraef, J. Lauzeral, and N.M. Ghoniem, *Phys. Rev. B* **53**, 14782 (1996).
17. P.A. Selischev and V.I. Sugakov, *Radiat. Eff.* **133**, 237 (1995).
18. V.O. Kharchenko and D.O. Kharchenko, *Eur. Phys. J. B* **85**, 383 (2012).
19. V.O. Kharchenko and D.O. Kharchenko, *Condens. Matter Phys.* **16**, 33001 (2013).
20. F.Kh. Mirzoev, V.Ya. Panchenko, and L.A. Shelepin, *Physics Uspekhi* **39**, 1 (1996).
21. L.A. Maksimov and A.I. Ryazanov, *Sov. Phys. JETP* **52**, 1170 (1980).
22. A.I. Olemskoi and A.Ya. Flat, *Phys. Solid State* **35**, 278 (1993).
23. V. Kharchenko and D. Kharchenko, *Phys. Rev. E* **89**, 042133 (2014).
24. J.W. Cahn and J.E. Hilliard, *J. Chem. Phys.* **28**, 258 (1958).
25. L.S. Darken, *Trans. AIME* **175**, 184 (1948).
26. A.M. Gusak, S.V. Kornienko, and G.V. Lutsenko, *Def. Diff. Forum* **264**, 109 (2007).
27. A.V. Nazarov and K.P. Gurov, *Fiz. Met. Metalloved.* **37**, 496 (1974).
28. K.P. Gurov and A.M. Gusak, *Fiz. Met. Metalloved.* **59**, 1062 (1985).
29. A.M. Gusak, T.V. Zaporozhets, Yu.O. Lyashenko, S.V. Kornienko, M.O. Pasichnyy, and A.S. Shirinyan, *Diffusion-Controlled Solid State Reactions in Alloys, Thin Films and Nanosystems* (Wiley-VCH, Berlin, 2010).
30. N.V. Tyutyunnyk and A.M. Gusak, *Ukr. Fiz. Zh.* **57**, 629 (2012).
31. R. Bullough and R.C. Newman, *Rep. Prog. Phys.* **33**, 101 (1970).
32. F.Kh. Mirzoev, V.Ya. Panchenko, and L.A. Shelepin, *Techn. Phys. Lett.* **22**, N 13, 28 (1996).
33. D.O. Kharchenko, S.V. Kokhan, and A.V. Dvornichenko, *Physica D* **238**, 2251 (2009).
34. D. Batogkh, M. Hildebrant, F. Krischer, and A. Mikhailov, *Phys. Rep.* **288**, 435 (1997).
35. D.O. Kharchenko, S.V. Kokhan, and A.V. Dvornichenko, *Metallofiz. Noveish. Tekhnol.* **31**, 23 (2009).
36. P.K. Galenko, D. Kharchenko, and I. Lysenko, *Physica A* **389**, 3443 (2010).

37. D. Kharchenko, I. Lysenko, and P.K. Galenko, in *Stochastic Differential Equations*, edited by N. Halidias (Nova Science, New York, 2011), p. 97.
38. D.O. Kharchenko, I.O. Lysenko, and V.O. Kharchenko, *Usp. Fiz. Met.* **13**, 1001 (2012).
39. D.O. Kharchenko, I.O. Lysenko, and S.V. Kokhan, *Eur. Phys. J. B* **76**, 37 (2010).
40. D. Kharchenko, I. Lysenko, and V. Kharchenko, *Physica A* **389**, 3356 (2010).
41. D.O. Kharchenko, I.O. Lysenko, and V.O. Kharchenko, *Ukr. J. Phys.* **55**, 1225 (2010).
42. R.A. Enrique and P. Bellon, *Phys. Rev. Lett.* **84**, 2885 (2000).
43. R.A. Enrique and P. Bellon, *Phys. Rev. B* **63**, 134111 (2001).
44. J.J. Hoyt and M. Haataja, *Phys. Rev. E* **83**, 174106 (2011).
45. A.D. Marwick, *J. Phys. F* **8**, 1849 (1978).

Received 06.05.15.

Translated from Ukrainian by O.I. Voitenko

*Д.О. Харченко, В.О. Харченко, А.І. Баштова*

САМООРГАНІЗАЦІЯ ВАКАНСІЙНОГО  
АНСАМБЛЮ ПРИ СПІНОДАЛЬНОМУ РОЗПАДІ  
БІНАРНИХ СИСТЕМ, ПІДДАНИХ СТАЛІЙ  
ДІЇ РАДІАЦІЙНОГО ОПРОМІНЕННЯ

Резюме

Розглянуто процеси перерозподілу нерівноважних вакансій при спінодальному розпаді бінарного твердого розчину, що знаходиться при сталій дії опромінення, в рамках узагальненої моделі Кана–Хілларда, яка враховує формування структурного безладу внаслідок опромінення. Виявлено, що зі збільшенням швидкості дефектоутворення процеси спінодального розпаду замінюються процесами формування просторових вакансійних структур. Встановлено, що формування кластерів вакансій супроводжується відбором структур. Досліджено кінетику розпаду та структуроутворення, статистичні розподіли полів концентрації розчину та концентрації вакансій за різних швидкостей набору дози опромінення.